Temperature Variation of DC Conductivity of Poly(3-alkyl Thiophenes) and Their Cocrystals

Susmita Pal, Somnath Roy, and Arun K. Nandi*

Polymer Science Unit, Indian Association for the Cultivation of Science, Jadavpur, Kolkata-700032, India

Received: April 22, 2005; In Final Form: July 23, 2005

The dc conductivity of poly(3-alkyl thiophenes) (P3ATs) and their cocrystals are measured in the temperature range of −130 to 150 °C. Both solvent-cast films and the melt-cooled films are used. The former exhibit a sharp increase followed by a decrease in conductivity, whereas the latter show only a sigmoidal increase in conductivity with temperature. The sigmoidal increase of the melt-cooled samples is dependent on the regioregularity and alkyl chain length of the samples and is explained from the solid-state transformation of the interdigited type-II crystal to a noninterdigited type-I crystal. The type-I crystal itself has lower conductivity than type-II crystals, and the samples exhibit a blue shift in UV−vis absorption spectra with an increase in temperature. So the sigmoidal increase of conductivity is attributed to the increase in carrier mobility with temperature in the type-I crystals. The X-ray and DSC results suggest that during the transformation of type-II to type-I crystals with increasing temperature, localized crystallites of smaller dimensions separated by narrower amorphous portions are produced throughout the whole matrix. But in the type-II polymorph, the crystallites are large with a wider gap in between. The sigmoidal increase is attributed to the easier hopping of the charge carrier among the localized crystallites of the type-I crystal with increasing temperature. In the cocrystals, the smaller sigmoidal increase with increasing irregular sample concentration is valid for a lower concentration of such localized crystallites. The same is true for cocrystals with longer alkyl chain lengths. The interfibrillar contribution of conductivity through the network junctions together with the carrier hopping between the localized crystallites might be a possible reason for the metallic-type behavior of solvent-cast samples after a certain temperature. The melt-cooled films do not exhibit metallic-type behavior because of the absence of a fibrillar network morphology.

Introduction

The transport properties of conducting polymers are commonly 1D and have been studied extensively.[1] Although high conductivity is reported for the doped conducting polymers, it decreases several orders of magnitude as the temperature is lowered.[2] This makes a difference in the conductivity mechanism from metal where conductivity rather increases with lowering of temperature. Among the conducting polymers poly(3-alkyl thiophenes) (P3ATs) are important members because they are easily processable and have very high conductivity in the doped state.[1,3] There are many reports on the conductivity of P3ATs.[1,3−10] Yoon et al. reported the conductivity of iodine-doped regioregular P3AT samples and obtained a maximum conductivity of 1170 s/cm for a poly(3-hexyl thiophene) (P3HT) sample.[4] They analyzed the conductivity versus temperature data in the temperature range of 1.3−200 K and concluded that samples having room-temperature conductivity <200 s/cm obey the 1D variable range hopping model according to the following equation

$$\sigma = \sigma_0 \exp - (T_0 / T)^{1/2} \qquad (1)$$

where σ_0 is a preexponential factor and T_0 is a characteristic temperature.

They also advocated that the exponent value of eq 1 changed progressively for samples of higher conductivity values (>200 S/cm) from 0.5 to 0.25, leading to a 3D hopping transport mechanism. Yoshino et al.[8] observed an anomalous temperature dependency of electrical conductivity of undoped regioirregular P3AT samples. The conductivity showed a maximum, and both the maximum conductivity and temperature decrease with an increase in alkyl chain length. The conductivity maximum was attributed to the molecular motion associated with the conformational change on the carrier scattering, which is dependent on the alkyl chain length, causing lower conductivity for higher alkyl chain length. Kowalik et al.[7] measured the dc conductivity of both regioregular and regioirregular poly(undecyl thiophene) and observed that the regioregular member has one order higher conductivity than that of the regioirregular sample. In addition, they observed a sharp increase in the conductivity of about three orders with an increase in temperature from −100 to +50 °C, and it is usually uncommon in normal semiconducting materials. Sirringhans et al.[9] studied the connectivity between the structure and conductivity of poly(3-alkyl thiophene) (P3AT) using X-ray diffraction. They determined from spectroscopic evidence that the charge carriers are 2D in nature and in the presence of strong $\pi-\pi$ interchain interaction the carriers are no longer confined to a single chain; rather, they have interchain character. Recently, Johansson and Larsson[10] showed from theoretical calculations that along the P3AT chains there is a wave packet localized over the five thiophene unit moving in the velocity determined essentially by the C−C stretching frequency. This is very different from metals in which the wave packet is mainly electronic and its velocity is determined by bandwidth.

* Corresponding author. E-mail: psuakn@mahendra.iacs.res.in.

10.1021/jp052093i CCC: $30.25
Published on Web 09/13/2005

P3ATs exhibit both solvatochromism and thermochromism that are attributed to two possible mechanisms: (i) intrachain mechanism and (ii) interchain mechanism.[12,13] The former is accompanied by backbone conformational changes or by side group disorder, and the latter is accompanied by crystallization, aggregation, induced rigidity, and so forth. Park and Levon[14] attributed the thermochromism of poly(3-dodecylthiophene) P3DDT films to the changes in chain conformation (intrachain mechanism) and also to crystallization of the sample (interchain mechanism). Thus, the thermochromism of P3DDT has been explained from the order−disorder transition of P3DDT chains, and similar reports of order−disorder transition are also observed for other regioirregular P3ATs in the literature.[15−17]

The crystal structure of P3ATs is interesting and has been worked out by many workers.[18−23] They are comblike polymers and produce an interchain lamellar structure in the solid state. In the crystalline state, two different types of crystalline structures are reported.[19,20] In the type-I crystal, the pendent alkyl groups of P3AT remain in the staggered conformation and they become tilted so that they remain in a hexagonal closed-pack structure. The overlapping of the side chains on the neighboring stack is minimal, although there is ordering of the side chain across the layer-to-layer interface. In type-II crystals, the interdigitation of side chains occurs, fully reducing the interchain lamellar thickness by ~30%. A schematic model of type-I and type-II structures for poly(3-octyl thiophene)-(P3OT) is shown in Scheme 1.[20] Type-I crystals are produced by casting the P3AT films rapidly (1−3 h) from the P3AT solution at high temperature, but type-II crystals are produced by slow casting (1−2 days) at room temperature. Rapid quenching of the samples from the melt also produced type-I crystals. The type-II structures are not stable, and modest heating of the interdigited (type-II) phase indicates a rapid solid-state transformation to the noninterdigited (type-I) phase.[20] In addition to the two crystalline phases, a mesophase of P3ATs is also reported.[22,23] This phase is characterized by a wide X-ray peak at $2\theta \approx 20°$ together with an interchain lamellar spacing of a type-I crystal and the absence of 3.8-Å intrastack chain-to-chain spacing.[23]

P3ATs produce cocrystals in the solid state,[11] and cocrystallization is an easy process to produce tailor-made properties (conductivity and optical properties) without having to use a much more laborious synthesis. However, the cocrystallization is limited to both the alkyl chain length difference and the head−tail (H−T) chain regioregularity. For the same alkyl chain length, cocrystallization is limited to a H−T regioregularity difference of 17 mol %; for the same regioregularity samples, it is limited to an alkyl chain length difference of two carbon atoms. The components with a varying alkyl chain length difference of two carbon atoms can cocrystallize for 7% difference of H−T regioregularity. The components crystallized in the same interchain lamella with intermediate lamellar thickness when cocrystallization occurred but in different lamellas in the absence of cocrystallization. The room-temperature dc conductivity of the samples was found to be either intermediate or lower than the line joining that of the components. In view of the potential applications of these materials in technology, the conduction mechanism of this polymer is to be explored. Any structural change that may occur with temperature would also affect the conductivity value and conduction mechanism. The conduction mechanism of the cocrystals is not yet known. In this paper, attempt will be made to delineate the conduction mechanism of the cocrystals as well as that of the pure components.

SCHEME 1: Approximate Molecular Model of Type-I and Type-II Poly(3-octyl Thiophene) Crystals

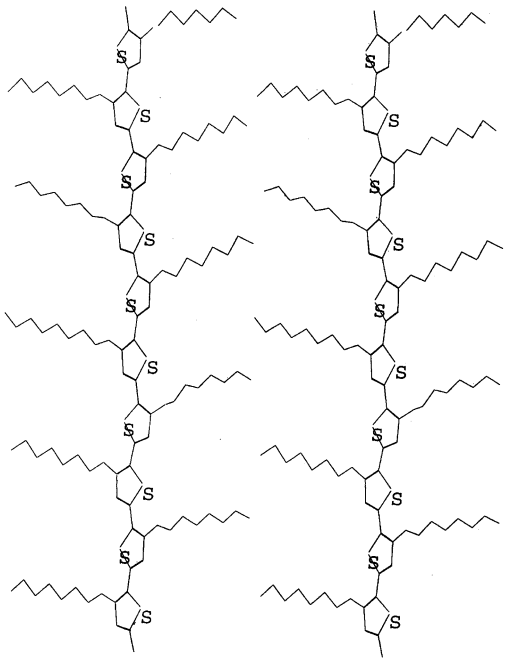

Non interdigited Type-I crystal (Staggered conformation)

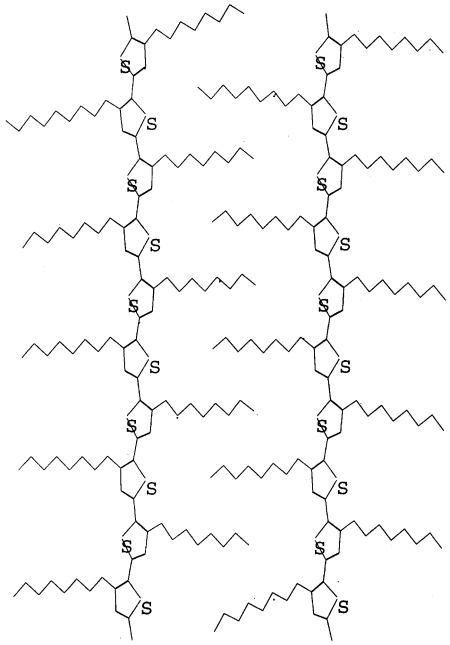

Interdigited Type-II crystal (Planar structure)

Experimental Section

A. Samples. Both regioregular and regioirregular P3AT samples were used in this work. Regioregular poly(3-hexyl thiophene) (P3HT-R) and poly(3-octyl thiophene) (P3OT-R) samples were purchased from Aldrich Chemical Co. As reported by the company, the samples were prepared by the method of Reike et al.[24] They were purified from suspended impurities by filtering with chloroform solution and then drying at 60 °C in a pull of air and finally in vacuum. The regioirregular samples were synthesized from the monomer 3-hexyl thiophene in $CHCl_3$ using anhydrous $FeCl_3$ as the initiator under nitrogen atmosphere.[25] The polymerization was carried out at +2 °C for the

TABLE 1: Characteristics of the Samples Used in this Work: Melting Point (T_m), Glass Transition Temperature (T_g) and β Transition Temperature (T_β) of Melt-Quenched Samples

P3AT samples	source	$\overline{M_W} \times 10^{-4}$	H−T regioregularity	T_m (°C)	T_g [a] (°C)	T_β [a] (°C)
P3HT(R)	Aldrich Chemical Co.	8.7	92	222	20.3	−101.2
P3OT(R)	Aldrich Chemical Co.	14.2	89	164	−9.2	−92.2
P3HT-1	prepared	8.7	75	161	1.8	−112.9
P3HT-2	prepared	10.6	82	182	18.1	−105.3

[a] See Supporting Information Figure 1. (T_g and T_β are the peak temperatures of the loss-modulus curves.)

first set and −5 °C for the second set. After 24 h of polymerization, the reaction mixtures were poured into methanol containing 10% HCl. The precipitate was redissolved in $CHCl_3$, and the filtrate was dried at 60 °C in air and finally in vacuum.

The molecular weights of the samples were measured from gel permeation chromatography using a μ-styragel column in tetrahydrofuran at 30 °C. Polystyrene samples were used as standards. The head to tail (H−T) regioregularity of the samples was measured from the ^{1}H NMR spectra[25] in a Bruker 300 MHz instrument using the peaks of α-carbon of 3-substituted thiophene. The characteristics of the samples are presented in Table 1.

Blends of the samples were prepared by mixing the two component polymers in different proportions in distilled chloroform and then evaporating to dryness at 60 °C in air and finally in vacuum for 3 days. Melt-cooled samples of the blends were prepared by melting the solvent-cast films in a Mettler (FP-82) hot stage and keeping them at a temperature 15 °C higher than the melting point of the higher melting component (Table 1) for 10 min under nitrogen atmosphere. They were then cooled in the hot stage under nitrogen atmosphere; it takes about 30 min to reach the 30 °C temperature.

B. Sample Characterization. The wide-angle X-ray scattering (WAXS) experiments were carried out in a Seifert X-ray diffractometer (C-3000) with a parallel beam optics attachment. The instrument was operated at a 35 kV voltage and a 30 mA current. Ni-filtered Cu Kα radiation has been used in this work. The samples were scanned from $2\theta = 2°$ to $2\theta = 40°$ at the step scan mode (step size 0.03°, preset time 2 s), and the diffraction pattern was recorded using a scintillation counter detector. The instrument was calibrated with a standard silicon sample before the run.

The melting point and enthalpy of fusion of the samples were measured using a differential scanning calorimeter (Perkin-Elmer, DSC-7). The samples were taken in aluminum pans and heated at a scan rate of 20°/min under nitrogen atmosphere. The melting point and enthalpy of fusion values were measured by a computer attached to the instrument using PC-series DSC-7 multitasking software (version 3.2). The instrument was calibrated with indium before each set of experiments. The scanning electron micrographs (SEM) of the films were taken from the gold-coated film using a Hitachi S-2300 scanning electron microscope.

C. DC Conductivity Measurement. The dc conductivities of the films were measured by the standard spring-loaded pressure contact four-probe method.[26] from −130 to 150 °C with an interval of 5 °C in vacuum. We developed an experimental setup with a heater in the sample holder. The holder was dipped into a sealed vacuum jar, which was cooled externally by a liquid nitrogen thermostat. Two separate programs were used to operate the whole system through a personal computer (PC): one for controlling the sample temperature and another for measuring the conductivity of the samples. The sample temperature was recorded by a thermocouple and was fed to PC via an analogue (A)/digital (D) input of an A/D−D/A card (PCL-207, Dynalog, India), and the temperature was controlled by the triggering of sample heater driving circuitry. A Keithley electrometer (model 617) and a Keithley digital multimeter (model 2000) were used as constant dc source and milivolt (mV) meter, respectively. The mV change was read by a digital multimeter and was fed to the PC via an RS 232 communication port for calculation of the conductivity.[27] Polymer films of ∼1.3 cm diameter were taken in the sample holder. They were kept at first at −130 °C, and then the temperature was increased to the next higher temperature using the heater in the sample holder. At each temperature, the sample was left for 5 min to attain thermal equilibrium. A constant current (I) was passed from the direct current source electrometer through two diagonal leads of four probes and the voltage (V) across the other two leads was measured using the digital multimeter. The conductivity (σ) was calculated using the van der Paw relation $\sigma = (\ln 2/\pi d)(I/V)$ where d is the thickness of the film.

Results

A. Solvent-Cast Samples. In Figure 1a−c, the representative plots of conductivity versus temperature of the solvent-cast films of cocrystals are presented and there is a maximum in each plot. Both the maximum conductivity and temperature (T_{max}) vary with the composition of the cocrystals. Figure 1a (and Supporting Information Figure 2a and b) indicates that the conductivity at particular temperature decreases with decreasing H−T regioregularity in the sample. Figure 1b also corroborates that at a particular temperature the conductivity of P3HT(R) is higher than that of the P3OT(R) sample, that is, it decreases with increasing alkyl chain length (because the H−T regioregularity in the two samples is almost same (Table 1)). In the cocrystals, conductivity decreases with increasing concentration of the lower melting component (P3OT(R)) and it is even lower than that of P3OT(R) in some compositions of the blend. This decrease might be occurring because of the larger insulating domains produced by the larger side chains.[28] In the case of P3OT(R)/P3HT(2) blends (Figure 1c), in which both regioregularity and alkyl chain length vary, conductivity, however, increased with increasing lower melting component except for the blend composition $W_{P3OT(R)} = 0.25$. The log conductivity versus temperature plots (Supporting Information Figure 3a−c) also show a maximum as in Figure 1a−c.

An interesting observation is that the conductivity rise is very sharp from 200 to about 350 K compared to the normal rise observed in semiconducting materials that usually follows eq 1.[1] Again, the sharp fall in conductivity after attaining the maximum value with increasing temperature is also interesting, and such a fall in conductivity is observed during the melting of polyaniline (PANI) gels.[27] The SEM micrographs (Figure 2a and b) of solvent-cast P3HT(R) and P3HT-1 films show a fibrillar network morphology. However, the decrease of con-

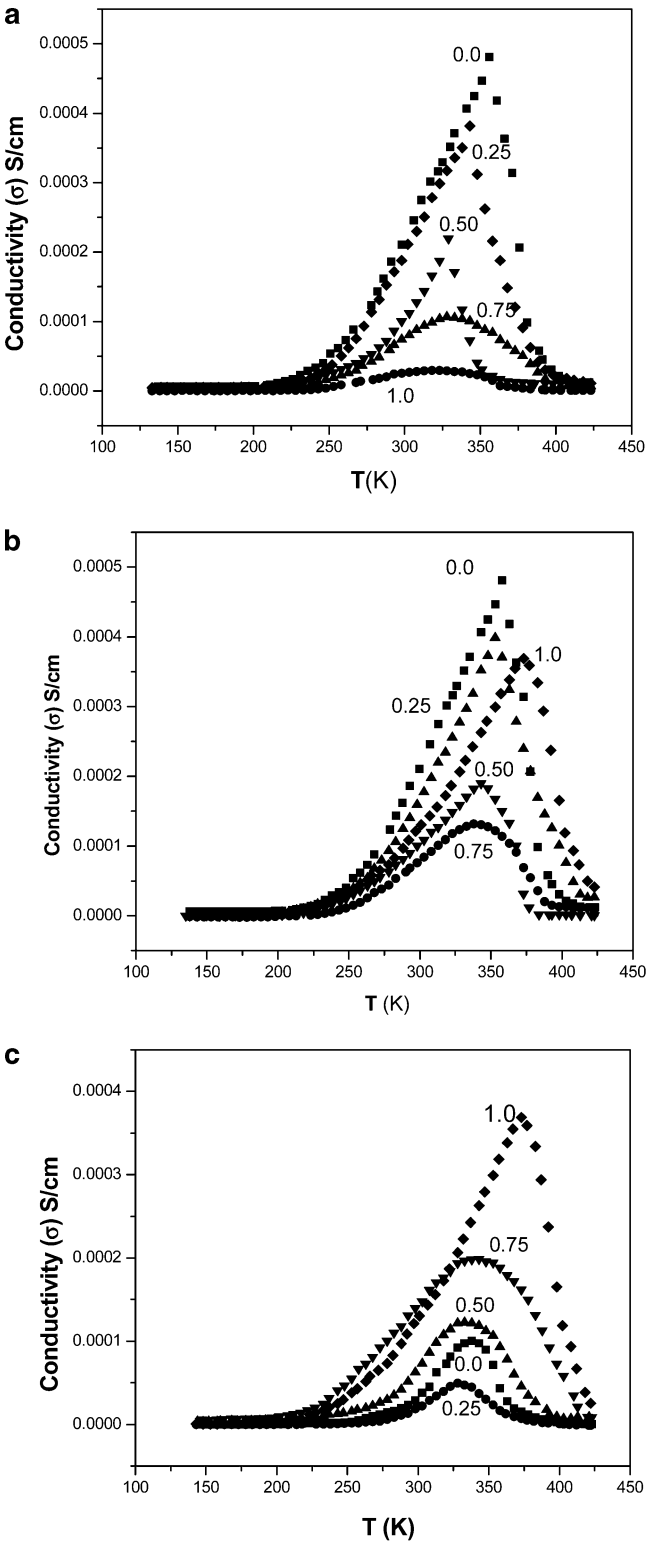

Figure 1. Conductivity vs temperature plot of solvent-cast films of P3ATs and their cocrystals: (a) P3HT(R)/P3HT-1 system, (b) P3HT-(R)/P3OT(R) system, and (c) P3OT(R)/P3HT-2 system. (The weight fractions of the lower melting component in the cocrystals are indicated in the Figures.)

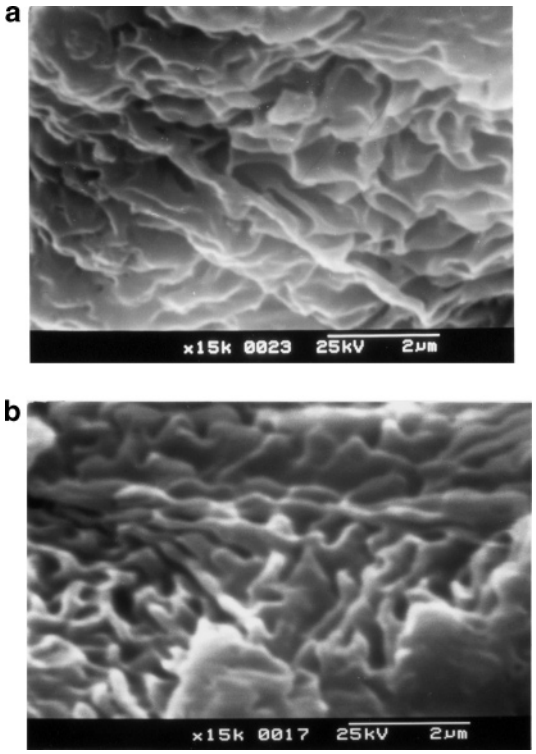

Figure 2. SEM pictures of P3AT films cast from chloroform solutions: (a) P3HT(R) and (b) P3HT-1.

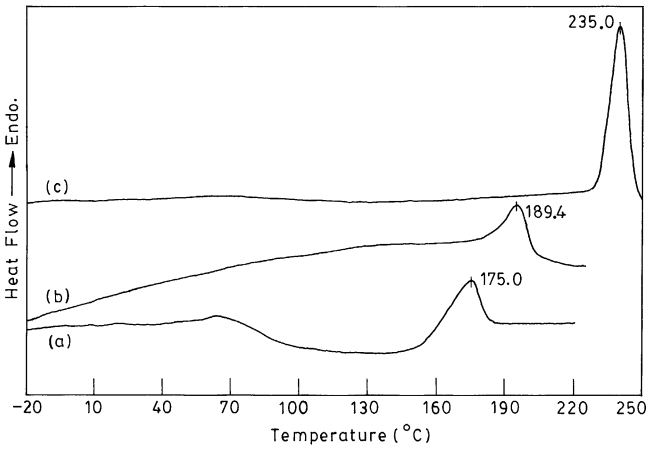

Figure 3. DSC thermograms of solvent-cast P3AT samples at the heating rate of 20 °C/min: (a) P3OT(R), (b) P3HT-1, and (c) P3HT-(R).

ductivity from the T_{max} might not be related to the melting of the network structure in this case because the DSC melting peaks (related to the melting of network structure) are at a much higher temperature (melting range: 175−235 °C; cf. Figure 3 and Table 2).[27] So conductivity due to both intrachain and interchain contribution exists even after T_{max}, and it might be possible that an insulator−metal type transition is occurring at T_{max} in the solvent-cast P3ATs and their cocrystals.

In Figure 4, plots of conductivity peak temperature with the weight fraction of the lower melting component are shown for all of the systems. In P3HT(R)/P3HT-1 and P3HT-1/P3HT-2 systems, the peak temperature decreases almost monotonically with increasing concentration of the lower melting component. However, in the other three systems, P3HT(R)/P3OT(R), P3OT-(R)/P3HT-2, and P3HT(R)/P3HT-2, the variation of the peak temperature is better represented by a concave upward curve. The conductivity peak temperature, which may be called an insulator−metal-like transition temperature, might be related to the structure of the cocrystals. The monotonic decrease may be explained by the fact that P3HT(R) and P3HT-1 produce cocrystals with the regioregularity being varied monotonically with the addition of P3HT-1. But the concave upward curves in the other systems might be due to the formation of cocrystals with a relatively larger amorphous portion, which decreases the

TABLE 2: Melting Peak Temperatures (°C) of Solvent-Cast Samples from DSC Thermogram

Weight fraction of the lower melting component	P3HT(R) + P3OT(R)	P3HT(R) + P3HT-1	P3HT(R) + P3HT-2	P3HT-1 + P3HT-2	P3OT(R) + P3HT-2
1.00	175.0	189.4	196.5	189.4	175.1
0.75	221.6	200.5	216.9	186.7	165.5
0.50	226.7	229.1	220.7	193.4	171.5
0.25	230.8	226.0	225.2	195.3	180.6
0.00	235.0	235.0	235.0	196.5	196.5

insulator−metal transition temperature, than the line joining that of the components.[11]

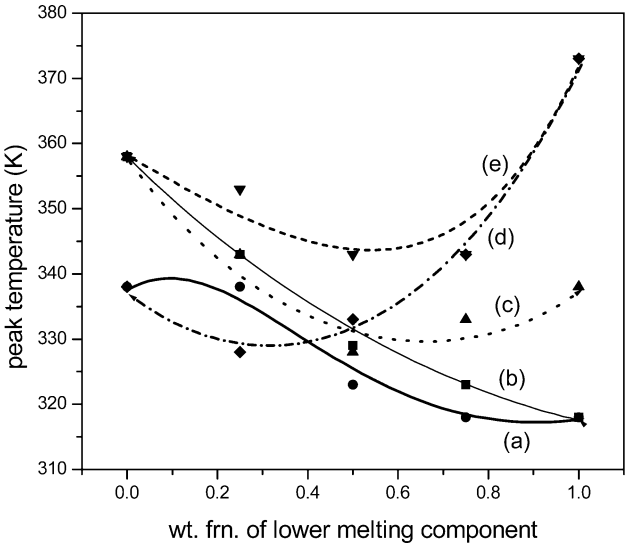

Figure 4. Peak temperatures of the conductivity plot of Figure 1 vs the weight fraction of the lower melting component: (a) P3HT-1/P3HT-2, (b) P3HT(R)/P3HT-1, (c) P3HT(R)/P3HT-2, (d) P3OT(R)/P3HT-2, and (e) P3HT(R)/P3OT(R).

Melt-Quenched Samples. In Figure 5 a−c, the conductivity of the melt-cooled samples are presented for different temperatures, and in every system a sigmoidal rise of conductivity with temperature is observed (see also Supporting Information Figure 4a and b). Here the nature of the plots is quite different from that of the solvent-cast samples (Figure 1a−c) because there is no maximum, rather, there is leveling at these temperatures in the plots. The log conductivity versus temperature plots also exhibit a similar sigmoidal rise (Supporting Information Figure 5a−c). This difference in behavior between the solvent-cast and melt-cooled films of P3AT is really interesting, and it may be due to some morphological effect. The SEM pictures of the melt-cooled samples, presented in Figure 6a−b, indicate no fibriller network structure as in the solvent-cast samples (cf. Figure 2). So, it may be argued that the metallic-type conductivity of solvent-cast films at higher temperatures than T_{max} arise from the fibrillar network morphology. Also, at a particular temperature the conductivity values of solvent-cast films are one order higher than that of the melt-cooled films. It may also be attributed to the additional interchain part of conductivity of the fibrillar network structure in the solvent-cast films.[6,27]

The origin of the sigmoidal increase of conductivity with increasing temperature will be evaluated in the following sections. Such a large variation of conductivity with temperature plot may not be due to the semiconducting behavior alone. This can be tested from the logarithmic variation of eq 1[29−31]

$$\ln W = \ln 1/2 + 1/2 \ln T_0 - 1/2 \ln T \qquad (2)$$

where $W = \delta \ln \sigma / \delta \ln T$.

Thus, a plot of ln W versus ln T should yield a negative slope of 0.5, but it yielded slope values of −6.4 and −5.5 (Figure 7a and b) for P3HT(R) and P3OT(R), respectively. This indicates that the sigmoidal increase is not due to semiconducting behavior alone and some other physical phenomenon is associated with these systems. Here we presume that some conformational transition of the polymer with temperature may take place as reported by others.[14,20] In P3ATs, the structural transition from type-II to type-I crystal and the order−disorder transition with increase in temperature is well known.[14,20] Such conformational changes yield some changes in the UV−vis spectra.[8,15,17] The UV−vis spectra of P3HT(R) and P3HT-1 samples at different temperatures are shown in Figure 8a and b for solvent-cast and melt-cooled films, respectively. Both figures indicate that there are blue-shifts, that is, the band gap has increased due to an increase in temperature, but it cannot account for the sigmoidal increase in conductivity of Figure 5. The conformational change with temperature produces a twist in the chain, decreasing the conjugation length and thereby increasing the band gap.[8,15,17] It is also noteworthy that in P3HT(R) solvent-cast films the two absorption peaks are distinct but the P3HT(1) film has single peak. The origin of the two peaks in the former case may be attributed to two different conjugation lengths in the sample,[16,24] whereas the P3HT(1) film has a single conjugation length. With an increase in temperature, the two peaks of the P3HT(R) solvent-cast film become closer gradually. In the melt-cooled samples, the two peaks of P3HT(R) are not resolved clearly as in the solvent-cast film. An isobestic point is observed clearly in the P3HT(1) sample for both the solvent-cast and melt-cooled state and also in the melt-cooled P3HT(R) films.[15,17] The coexistence and interconversion of the short-range ordered structure dispersed in the disordered bulk phase have been attributed to the observed isobestic point.[17]

A question may arise regarding the onset temperature of the conductivity jump, which is ∼200 K for the regioregular samples. However, the measured T_g values of the samples are really high (Table 1). Apparently such conformational transitions are unfavorable at this low temperature (−73 °C). P3ATs are comblike polymers, and there are two types of motion: side-chain motion and the segmental movement of the main thiophene chain. The side-chain movement is characterized by the β-transition temperature (T_β), and the main chain segmental motion is characterized by the glass transition temperature. The T_β values of P3ATs are at ∼ −100 °C (Table 1). Consequently, the side-chain motions may take place at 200 K and are probably the reason for the above onset in conductivity rise. It is now known that the type-II P3AT crystals convert to type-I crystals by increasing the temperature.[20,23] Type-II crystals are fully interdigited, and the interchain lamella is planar. But in type-I crystals, the side chains are staggered and not interdigited (Scheme 1). So it may be proposed that because of the movement of the side chains the interdigited type-II structure transforms gradually into a noninterdigited type-I structure in the solid state.

To study this phenomenon, we made X-ray investigations of a P3HT(R) film cooled from melt to 30 °C at the hot stage

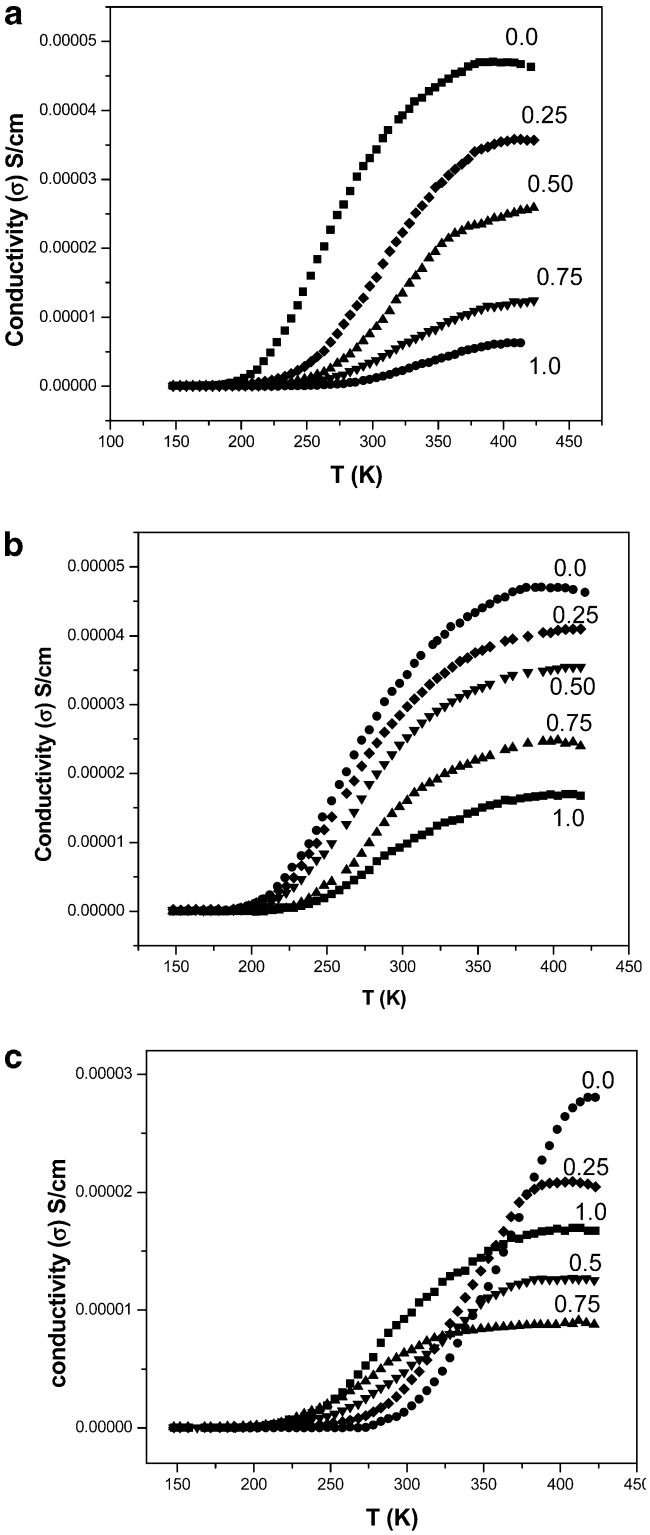

Figure 5. Conductivity vs temperature plot of melt-cooled samples (in hot stage) and their cocrystals: (a) P3HT(R)/P3HT-1 system, (b) P3HT(R)/P3OT(R) system, and (c) P3OT(R)/P3HT-2 system. (The weight fractions of the lower melting component in the cocrystals are indicated in the Figures.)

under nitrogen atmosphere and the same film annealed at 110 °C for 16 h and then quenched to room temperature. The results are shown in Figure 9; the X-ray patterns are somewhat different in the two cases. The melt-cooled specimen produces a large peak at $2\theta = 5.4°$ and small peaks at $2\theta = 10.5$ and 23.7°. The former corresponds to the interchain lamellar peak with a

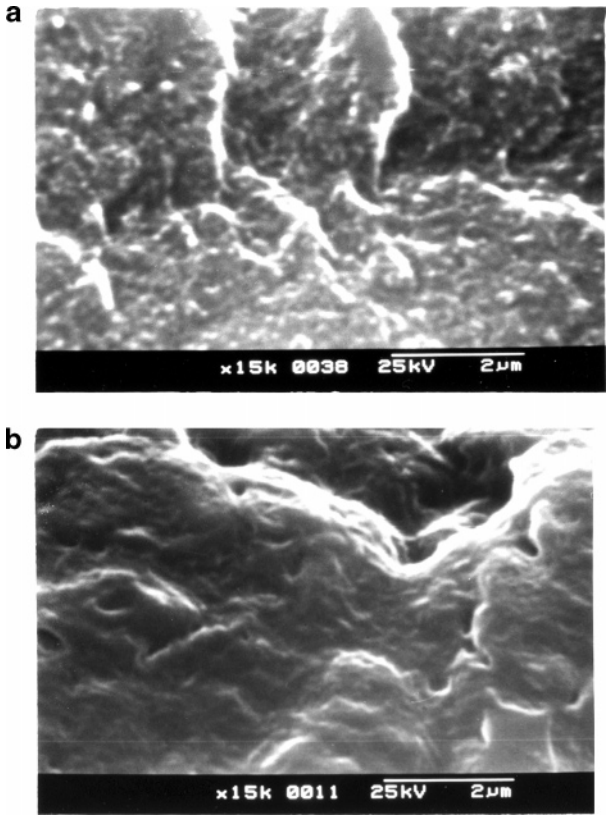

Figure 6. SEM pictures of P3AT films produced by melt-cooled method in Metler hotstage: (a) P3HT(R) and (b) P3HT-1,

lamellar distance of 16.3 Å. But the same sample annealed at 110 °C for 16 h showed a large peak at $2\theta = 5.1°$ for an interchain lamella thickness of 17.6 Å. So compared to that of the former crystal, there is an 8% increase in lamellar thickness. In literature, two types of crystalline polymorphs (type-I and type-II) and a mesomorph are reported for P3OT, poly(3-dodecyl thiophene)(P3DDT), and poly(3-decyl thiophene) (P3DT).[20,22,23] However, to our knowledge no WAXS pattern of a type-II polymorph of P3HT is reported. We presume that the X-ray diffractogram, part a of Figure 9, originates from that of a type-II polymorph of P3HT and has been partially converted to a type-I polymorph. This is probably because the type-II polymorph of P3HT is not stable at room temperature (30 °C), and it rapidly transforms into more stable type-I polymorph (cf. following sections). The diffractogram (part a) has been assigned to the partially transformed type-I polymorph from the type-II polymorph because the nature is almost the same for the type-I polymorph but the lamellar distance is 8% shorter than that of the type-I polymorph. Also, the sharp melting peak of the melt-cooled sample (Figure 10 a) supports that the diffractogram (part a) of Figure 9 is not for a mesophase; rather, it represents a crystalline polymorph. By annealing at 110 °C, we find that it converts completely into a noninterdigitated nonplanar type-I polymorph (diffractogram b).[20,22,23] The DSC thermogram (Figure 10) of the melt-cooled samples indicates a melting point of 223.1 °C and an enthalpy of fusion of 17 J/g, whereas the same sample kept at 110 °C for 16 h and quenched to 50 °C showed a melting peak of 219.3 °C and an enthalpy of fusion of 17 J/g. Such an observation is unusual in crystalline polymers in which annealing increases the melting point. The decrease in melting point may be attributed to the transformation into a less densely packed crystal arising from the decreased interdigitation (i.e., increased lamellar thickness) of the side chains.

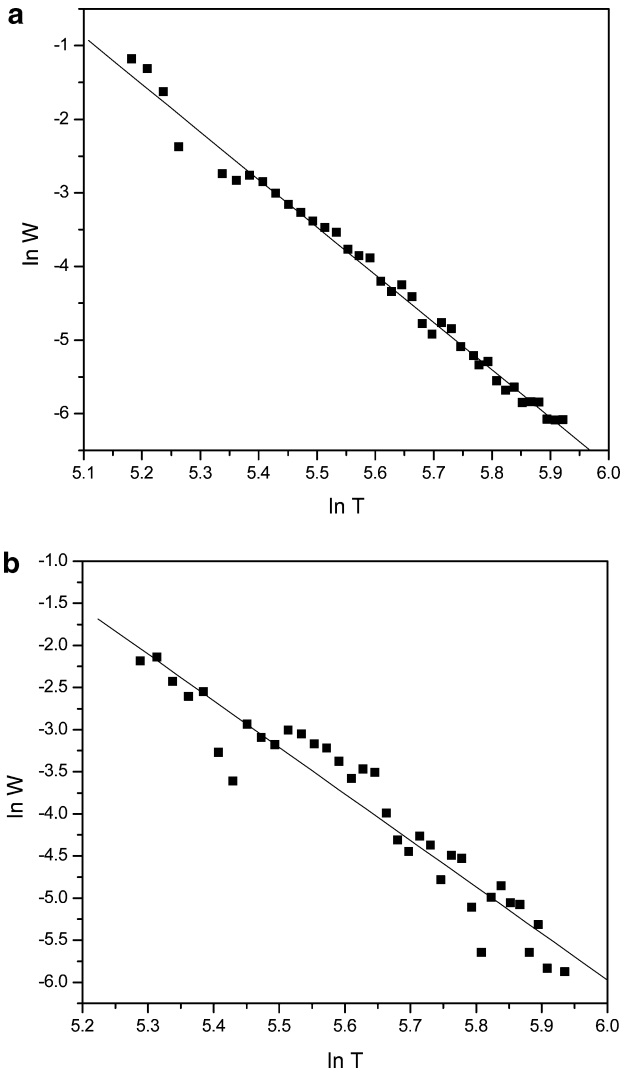

Figure 7. ln *W* vs ln *T* plot of the conductivity data of the (a) P3HT-(R) and (b)P3OT(R) systems.

This DSC result also provided evidence that the sample produced under the melt-quenched state is a type-II crystal rather than a mesomorph.

It is now pertinent to determine whether the transition from a type-II to a type-I crystal can occur at room temperature (30 °C) because both T_β and T_g are lower than room temperature. The X-ray patterns of the melt-cooled sample after keeping it at room temperature for different lengths of time are presented in Figure 11. A gradual change in the X-ray pattern with annealing time from partially transformed type-II to type-I crystal is observed. So the present study concludes that the planar type-II P3AT crystal transforms gradually into a non-planar type-I crystal for annealing at room temperature. It is necessary to mention here that during X-ray measurements after cooling the samples at room temperature it took about an hour to run the data. So the X-ray diffractogram shown here does not correctly represent that of the melt-cooled sample, rather, after annealing of 1 h at room temperature. At this time, the type-II to type-I conversion becomes more than 50% complete (cf. conductivity data in the discussion section). In our present setup, we cannot minimize the waiting time to run the X-ray and this problem will be critically addressed later by a synchrotron radiation experiment. However, at lower annealing temperatures the conformational transition rate may be lower.

Discussion

The conductivity in conducting polymers is generally determined by carrier density and carrier mobility. The carrier density depends on the band gap and impurity level.[8] In the same sample, the impurity level is same. So the temperature dependency of conductivity depends only on the temperature dependency of the band gap. The band gap can be evaluated from the absorption peak in the UV−vis spectra (Figure 8a and b). The blue shift of the $\pi-\pi^*$ absorption band of P3HT(R) with increasing temperature indicates that the band gap of P3HT(R) increases with temperature. So the carrier density has decreased with an increase in temperature. The increase of conductivity at the sigmoidal region is therefore due to the increase of carrier mobility, which depends on morphology, crystallinity, and so forth. Sirringhaus et al. observed efficient interchain transport in 2D (planar) conjugated lamella of P3HT. So, the conductivity of the type-II P3HT crystal will be higher than that of the noninterdigited (nonplanar) type-I crystal. In Figure 12, the conductiivity of the type-II crystal is found to decrease with time and finally it becomes fixed at ∼4 h. This drop in conductivity is in accordance with the view of Sirringhaus et al.[9] as type-I crystals are produced with time from type-II crystals (cf. Figure 11). So the cause of the sigmoidal increase of conductivity still remains unsolved. It should be noted here (from Figure 12) that at about 1 h of annealing more than 50% conversion of the type-II into the type-I polymorph is complete.

P3ATs are semicrystalline polymers (crystallinity 10−15%),[32] and the crystalline domains are embedded within the amorphous matrix.[33] The amorphous matrix has a lower charge carrier mobility than that of the crystalline matrix.[9] So increased crystallinity and a good dispersion of crystalline domains may yield such an increase in conductivity. In Figure 13, DSC thermograms of samples of approximately the same thermal history as in the conductivity experiments (Figure 5) are presented. There is a decrease in the melting point from 225.9 to 219.8 °C as we annealed the samples from lower to higher temperature. The enthalpy of fusion also decreases as 19.8, 19.6, 16.9, and 15.7 J/g with increasing annealing temperature in Figure 13. The higher crystallinity in type-II crystals is due to the higher side-chain interdigitation, and such interdigitation makes the crystallite size larger, yielding a higher melting point.[33] At a higher annealing temperature, the type-II form of P3HT transforms completely into a type-I polymorph. The lower crystallinity and lower melting point of the type-I P3HT crystal might be due to the lesser overlapping of side chains arising from the staggered conformation of the hexyl side chains. Now it is interesting to compare the X-ray patterns of the partially transformed type-I polymorph from type-II and type-I crystals (Figure 9 and Figure 11). Both crystals have very prominent crystalline diffraction peaks. These results are somewhat different from the above DSC observation where type-II crystals have a much higher melting point and enthalpy of fusion. One possible explanation is that the size of the type-I crystal domains are smaller and such domains are larger in number than those of the type-II crystals. The smaller crystallites have lower melting points and lower enthalpies of fusion.[33] The sharper X-ray patterns with lower amorphous intensity in the type-I crystal is due to the fact that X-ray can recognize all of the small crystallites and yields a cumulative diffraction pattern for all of the crystallites. So the overall X-ray crystallinity of the type-I crystal is found to be somewhat higher (27%) compared to the X-ray crystallinity of type-II transformed type-I crystals (20%). These results, therefore, indicate the increased formation of a large number of small-size type-I crystallites (localized

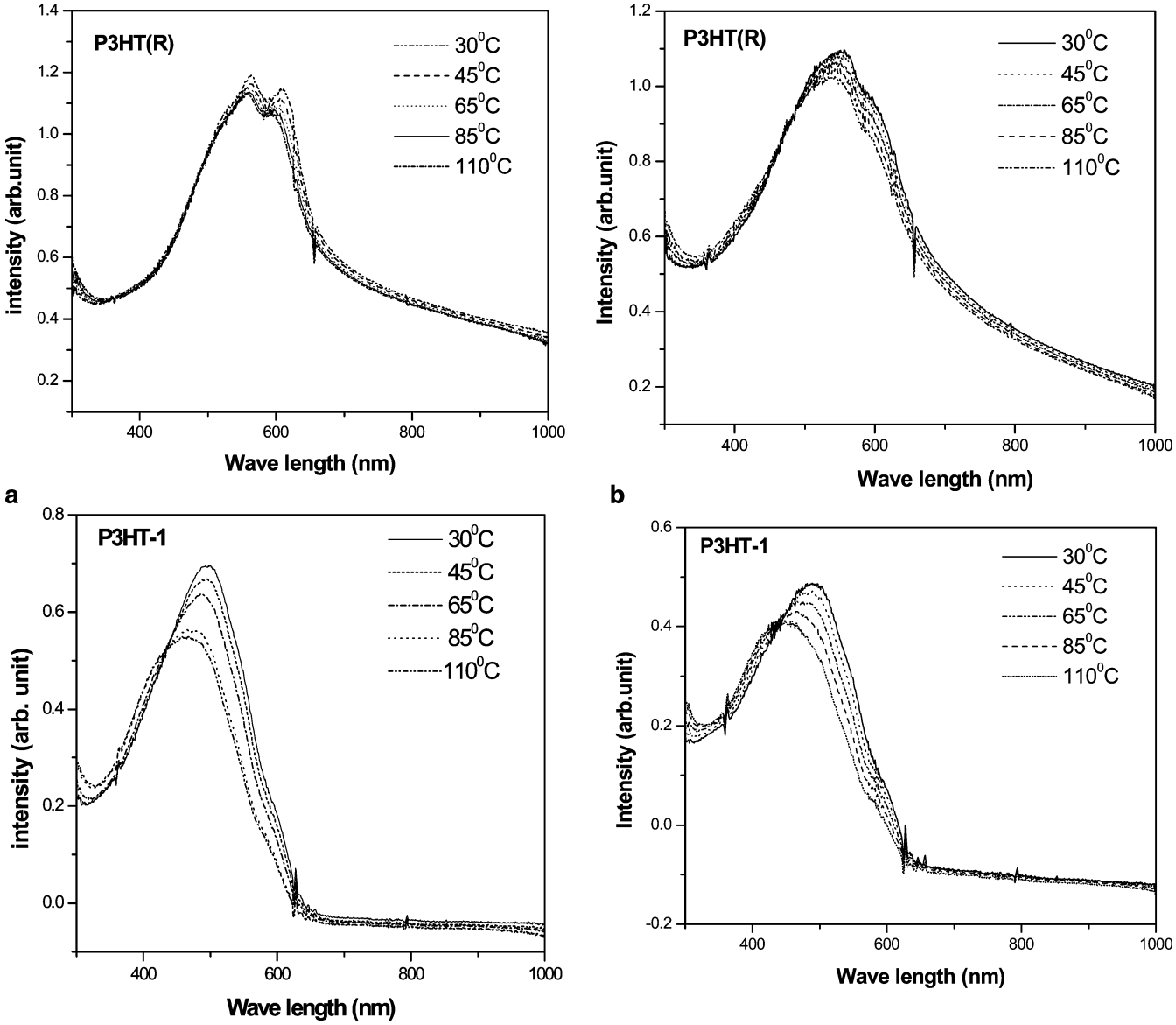

Figure 8. (a) Temperature variation of UV−vis spectra for P3HT(R) and P3HT-1 solvent-cast films at indicated temperatures. (b) Temperature variation of UV−vis spectra of P3HT(R) and P3HT-1 melt-cooled film in hot stage at indicated temperatures.

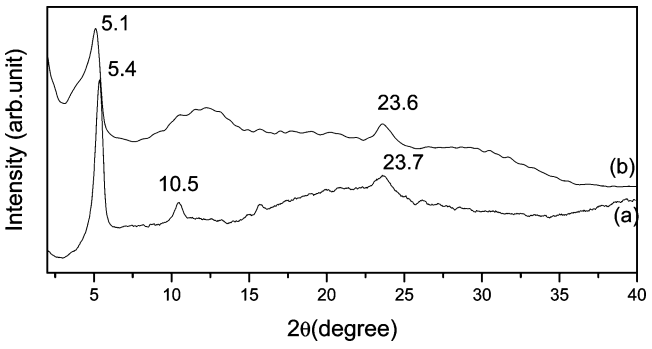

Figure 9. WAXS pattern of P3HT(R) film. (a) Melt-cooled in hot stage (b) the same film annealed at 110 °C for 16 h and quenched to 30 °C.

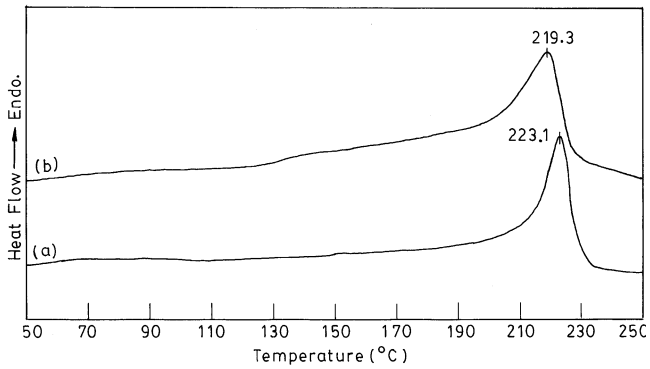

Figure 10. DSC thermograms of (a) melt-cooled P3HT(R) sample and (b) the same sample annealed at 110 °C for 16 h and quenched to 50 °C in DSC at the heating rate of 20 °C/min.

structure) during the increase of temperature. Schematic models of crystallite distribution of type-I and type-II crystals are given in Figure 14.

To understand the sigmoidal rise in conductivity of P3HT-(R) with temperature, one may use the above schematic diagrams. In type-II crystals, the large crystalline domains are well separated by the noncrystalline domains of P3AT. With increasing temperature, the carrier mobility by the hopping process is not increased much because of the wide amorphous barrier. But in type-I P3AT crystals, the crystalline domains are separated by narrower amorphous portions of P3AT; consequently, with increasing temperature carrier hopping is easier because a small amount of thermal energy is gained and

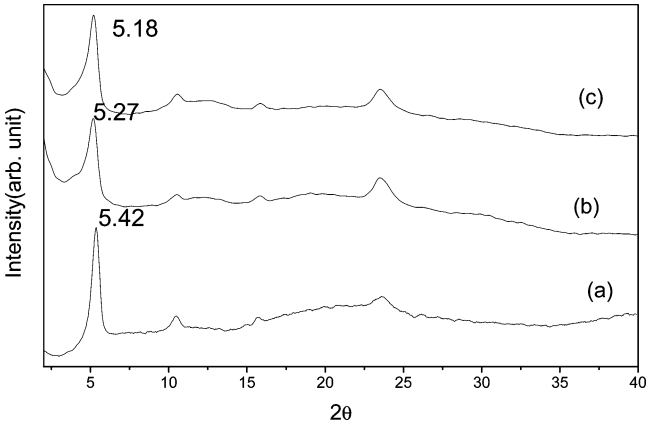

Figure 11. WAXS pattern of the melt-cooled P3HT(R) film annealed at 30 °C for different times. (a) Melt-cooled film, (b) 7 h, and (c) 12 h.

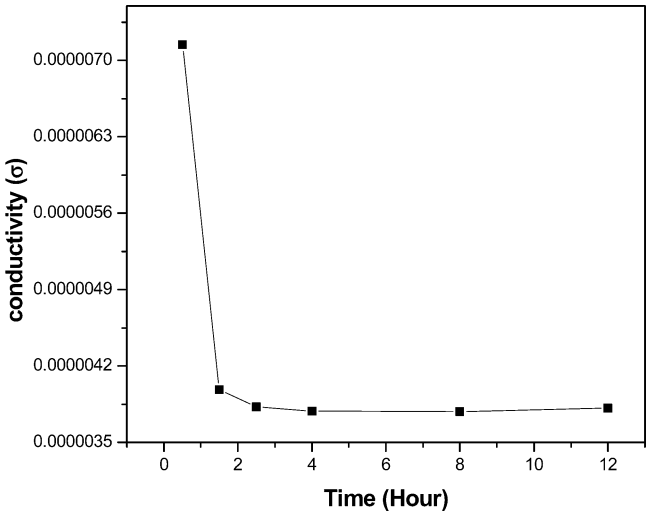

Figure 12. Conductivity vs time plot of the melt-cooled P3HT(R) sample annealed at 30 °C.

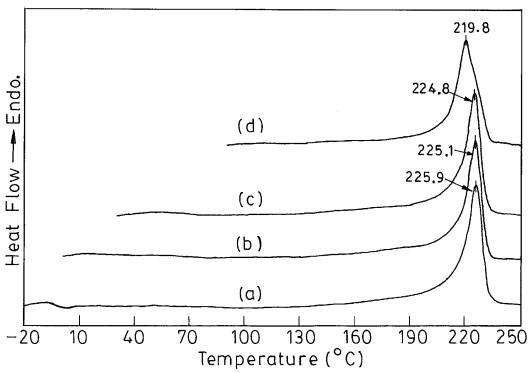

Figure 13. DSC thermograms of the melt-cooled P3HT(R) sample kept at different temperatures as in the conductivity−temperature experiment (Figure 5): (a) −30 °C for 10 min, (b) 0 °C for 30 min, (c) 30 °C for 1 h, and (d) 90 °C for 1.5 h (heating rate 20°/min).

this causes the sigmoidal increase in conductivity as type-I crystals are produced progressively. When the formation of such small crystalline domains is complete, an almost leveling of conductivity with increasing temperature is observed. Thus, the sigmoidal increase in conductivity of P3AT with temperature may be explained.

The relative sigmoidal rise of conductivity in the cocrystals of Figure 5a−c may be explained in a similar fashion. The regioirregular chains have lower conductivities and the conductivity rise with temperature is also low because of the larger number of defect structures present in the chain. The larger amount of head-to-head defect in the P3AT chain of the regioirrregular samples may prohibit the formation of localized small crystallites because of conformational restriction. The percentage of regioregular chains in a mixture of regioregular

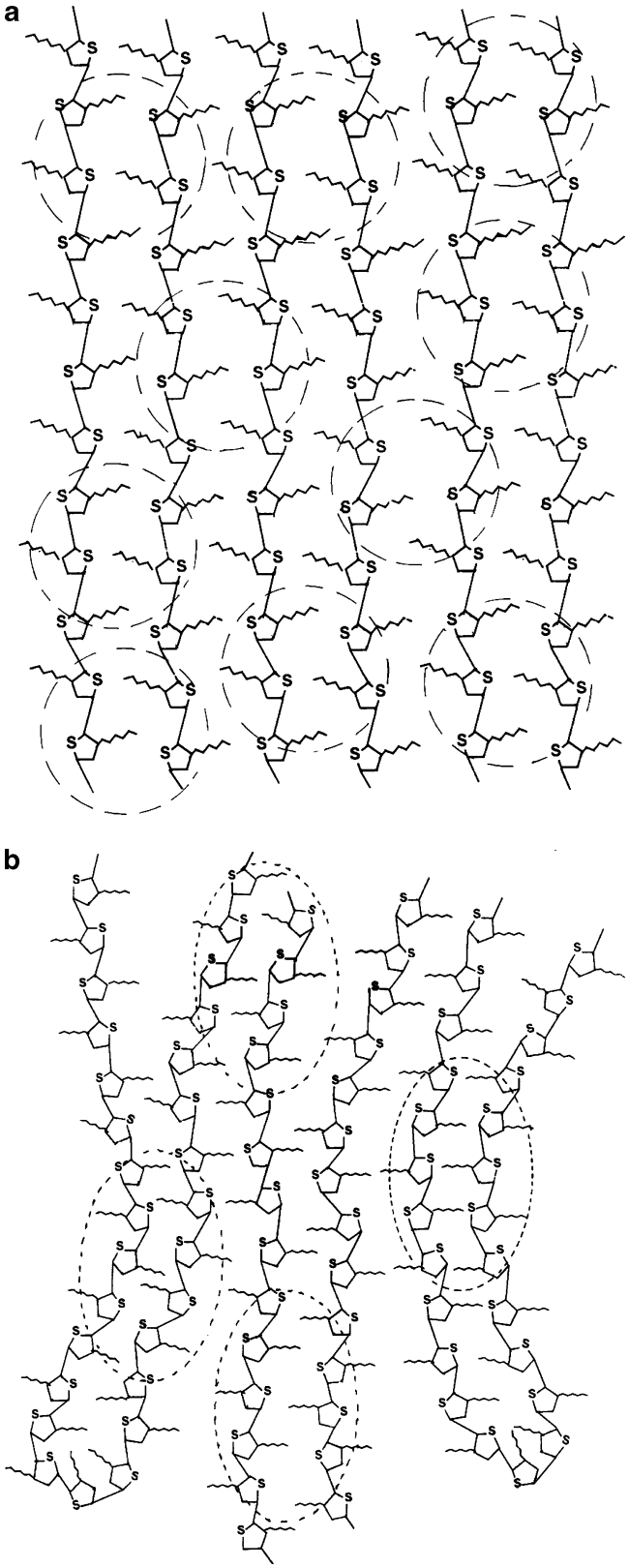

Figure 14. Schematic presentation of the distribution of crystallites of (a) P3HT type-I and (b) P3HT type-II crystals (the dotted circle indicates the crystallite portions and the rest is the amorphous matrix).

and regioirregular samples controls the formation of such a localized small crystalline structure, and the higher the percentage of irregular chains the lower the amount of localized structure. Consequently, the height of the sigmoidal increase of conductivity decreases with increasing of the regioirregular component. In the case of P3OT(R), the twisting of side chains is more difficult than with P3HT(R) because of the larger size of the side chain (cf. T_β values of Table 1). So, the formation of the localized crystalline domains is lower and the sigmoidal rise in conductivity is lesser when compared to P3HT(R). In its cocrystals, the effect will be similar to that discussed in the case of the cocrystals of the P3HT(R)/P3HT-1 samples.

In solvent-cast samples, the same type-II to type-I crystal transformation occurred. During the transformation, it produced localized small-size crystallites in which hopping of charge carrier is easily possible with an increase in temperature. This gives a sharp increase of conductivity with temperature, but from the temperature where transformation is complete it shows metallic behavior (Figure 1a−c). No definite reason for this metallic-type behavior is known, and the fibrillar network structure of the solvent-cast film may be the reason for such metallic-type behavior. A similar metallic-type behavior of conductivity was also observed in some polyaniline−surfactant gels.[27] Apart from the hopping between localized crystalline domains, the additional conduction from the interfibrillar region through the network junctions made the solvent-cast films metallic-type. In the cocrystals with lower regioregular content, the metal−insulator-type transition is found to be low and also occurred at a lower temperature. This is probably due to the lower concentration of the localized crystallite structure for lower regioregular samples.

Conclusions

The temperature variation of conductivity of P3AT samples is very interesting. Solvent-cast films from chloroform show different behavior than that of the melt-cooled samples. The solvent-cast films show a sharp increase followed by a decrease, whereas the melt-cooled films show only a sigmoidal increase. The sigmoidal increase in conductivity with temperature has been attributed to the solid-state transformation of interdigited type-II crystals into noninterdigited type-I crystals. Although the conductivity of the type-I crystal is low, the sigmoidal rise in conductivity has been attributed to the formation of smaller-size but well-dispersed crystalline regions. The carrier hopping between the crystalline domains with temperature is easier in type-I crystals than in type-II crystals where they are separated by wider amorphous portions of P3AT. The decrease in conductivity of solvent-cast films after the maximum has been attributed to the metallic-type behavior arising from the larger concentration of localized crystalline domains together with the conduction from interfibrillar part through the network junctions.

Acknowledgment. We gratefully acknowledge CSIR grant no. 1919/04/EMR-II for financial support.

Supporting Information Available: Conductivity versus temperature plots of various samples. This material is available free of charge via the Internet at http://pubs.acs.org.

References and Notes

(1) Mennon, R.; Yoon, C. O.; Moses, D.; Heeger, A. J. In *Handbook of Conducting Polymers*, 2nd ed.; Skotheim, T. A., Elsenbaumer, R. L., Renolds, J. R., Eds.; Marcel Dekker: New York, 1998; p 27.

(2) Menon, R.; Yoon, C. O.; Moses, D.; Heeger, A. J. *Phys. Rev. B* **1993**, *47*, 1758.

(3) (a) Roncali, J. *Chem. Rev.* **1992**, *92*, 711. (b) McCullough, R. D.; Ewbank, P. C. In *Handbook of Conducting Polymers*, 2nd ed.; Skotheim, T. A., Elsenbaumer, R. L., Renolds, J. R., Eds.; Marcel Dekker: New York, 1998; p 225.

(4) Yoon, C. O.; Reghu, M.; Moses, D.; Heeger, A. J.; Cao, Y.; Chen, T.-A.; Wu, X.; Reike, R. D. *Synth. Met.* **1995**, *75*, 229.

(5) Sinou, B.; Pepin-Donat, B.; Nechtschein, M. *Polymer* **1997**, *38*, 1581.

(6) Malik, S.; Jana, T.; Nandi, A. K. *Macromolecules* **2001**, *34*, 275.

(7) Kowalik, J.; Tolbert, L. M.; Narayan, S.; Abhiraman, A. S.; *Macromolecules* **2001**, *34*, 5471.

(8) Yoshino, K.; Park, D. H.; Park, B. K.; Fujii, M.; Sugimoto, R-i. *Jpn. J. Appl. Phys.* **1988**, *27*, L1410.

(9) Sirringhaus, H.; Brown, P. J.; Friend, R. H.; Neilsen, M. M.; Bechgaard, K.; Langeveld-Voss, B. M. W.; Spiering, A. J. H.; Janssen, R. A. J.; Meijer, E. W.; Herwig, P.; de Leeuw, D. M. *Nature* **1999**, *401*, 685.

(10) Johansson, E.; Larsson, S. *Synth. Met.* **2004**, *144*, 183.

(11) (a) Pal, S.; Nandi, A. K. *Macromolecules* **2003**, *36*, 8426. (b) Pal, S.; Nandi, A. K. *J. Phys. Chem. B* **2005**, *109*, 2493.

(12) Rughooputh, S. D. D. V.; Hotta, S.; Heeger, A. J.; Wudl, F. *J. Polym. Sci. Part B: Polym. Phys.* **1987**, *25*, 1071.

(13) Inganas, O.; Salaneck, W. R.; Osterholm, J. E.; Lakkaso, J. *Synth. Met.* **1988**, *22*, 395.

(14) Park, K. C.; Levon, K. *Macromolecules* **1997**, *30*, 3175.

(15) Faid, K.; Frechette, M.; Ranger, M.; Mazerolle, L.; Levesque, I.; Leclerc, M.; Chen, T. A.; Reike, R. D. *Chem. Mater*. **1995**, *7*, 1930.

(16) McCullough, R. D.; Low, R. D.; Jayaraman, M.; Anderson, D. *J. Org. Chem.* **1993**, *58*, 904.

(17) Yang, C.; Orfino, F. P.; Holdcroft, S. *Macromolecules* **1996**, *29*, 6510.

(18) Tashiro, K.; Ono, K.; Minagawa, Y.; Kobayashi, M.; Kawai, T.; Yoshino, K. *J. Polym. Sci.* **1991**, *B29*, 1223

(19) Prosa, T. J.; Winokur, M. J.; Moulton, J.; Smith, P.; Heeger, A. J. *Macromolecules* **1992**, *25*, 4364.

(20) Prosa, T. J.; Winokur, M. J.; McCullough, R. D. *Macromolecules* **1996**, *29*, 3654.

(21) Tashiro, K.; Kobayashi, M.; Kawai, T.; Yoshino, K. *Polymer* **1997**, *38*, 2867.

(22) Meille, S. V.; Romita, V.; Caronna, T.; Lovinger, A. J.; Catellani, M.; Belobrzeckaja, L. *Macromolecules* **1997**, *30*, 7898

(23) Bolognesi, A.; Porzio, W.; Zhuo, G.; Ezquerra, T. *Eur. Polym. J.* **1996**, *32*, 1097.

(24) Chen, T.-A.; Wu, X.; Rieke, R. D. *J. Am. Chem. Soc.* **1995**, *117*, 233.

(25) Amou, S.; Haba, O.; Shiroto, K.; Hayakawa, T.; Ueda, M.; Takeuchi, K.; Asai, M. *J. Polym. Sci, Polym. Chem. Ed.* **1999**, *37*, 1943.

(26) Frommer, J. E.; Chance, R. R. In *Encyclopedia of Polymer Science and Engineering*, 2nd ed.; Menges, G., Mark, H.-F., Bikales, N. M., Overberger, C. G, Eds.; John Wiley and Sons: New York, 1986; Vol. 5, p 473.

(27) Jana, T.; Roy, S.; Nandi, A. K. *Synth. Met.* **2003**, *132*, 257.

(28) Ding, L.; Lu, Z.; Egbe, D. A. M.; Karasz, F. E. *Macromolecules* **2004**, *37*, 10031

(29) Dutta, P.; Biswas, S.; Ghosh, M.; De, S. K.; Chatterjee, S. *Synth. Met.* **2001**, *122*, 455.

(30) Kim, B. H.; Jung, J. H.; Kim, J. W.; Choi, H. J.; Joo, J. *Synth. Met.* **2001**, *117*, 115.

(31) Yoon, C. O.; Reghu, M.; Moses, D.; Heeger, A. J.; Cao, Y. *Synth. Met.* **1994**, *63*, 47.

(32) Malik, S.; Nandi, A. K. *J. Polym. Sci., Polym. Phys. Ed.* **2002**, *40*, 2073.

(33) Mandelkern, L. In *Comprehensive Polymer Science*; Allen, G. Ed.; Pergamon Press: Oxford, 1989; Vol. 2, p 363.